ICARUS 33, 186–202 (1978)

Analysis of Stellar Occultation Data

Effects of Photon Noise and Initial Conditions

R. G. FRENCH, J. L. ELLIOT, AND P. J. GIERASCH

Laboratory for Planetary Studies, Center for Radiophysics and Space Research, Cornell University, Ithaca, New York 14853

Received December 23, 1976; revised June 7, 1977

A new inversion technique for obtaining temperature, pressure, and number density profiles of a planetary atmosphere from an occultation light curve is described. This technique employs an improved boundary condition to begin the numerical inversion and permits the computation of errors in the profiles caused by photon noise in the light curve. We present our assumptions about the atmosphere, optics, and noise and develop the equations for temperature, pressure, and number density and their associated errors. By inverting in equal increments of altitude, Δh, rather than in equal increments of time, Δt, the inversion need not be halted at the first negative point on the light curve as required by previous methods. The importance of the boundary condition is stressed, and a new initial condition is given. Numerical results are presented for the special case of inversion of a noisy isothermal light curve. From these results, simple relations are developed which can be used to predict the noise quality of an occultation. It is found that fractional errors in temperature profiles are comparable to those of pressure and number density profiles. An example of the inversion method is shown. Finally, we discuss the validity of our assumptions. In an appendix we demonstrate that minimum fractional errors in scale height determined from the inversion are comparable to those from an isothermal fit to a noisy isothermal light curve.

I. INTRODUCTION

Observations of stellar occultations by planets have been used to obtain temperature and number density profiles of the occulting planet's atmosphere, through the numerical inversion of the light curve (Kovalevsky and Link, 1969; Hubbard *et al.*, 1972; Vapillon *et al.*, 1973; Veverka *et al.*, 1974). An objection to this technique for reducing occultation data is that there has been no way of associating quantitative uncertainties with the results of the inversion. The uncertainties are of two types. First, the assumptions concerning the planetary atmosphere necessary to do the inversion calculation may not be valid (Young, 1976; Elliot and Veverka, 1976; Jokipii and Hubbard, 1977). Second, the photometric errors affecting the light curve—photon noise, terrestrial scintillation, and baseline uncertainties, for example —must necessarily propagate into the temperature and number density profiles, but these effects have not been evaluated with any generality (Hubbard *et al.*, 1972; Wasserman and Veverka, 1973; Hunten and Veverka, 1976).

In this paper we present a method for calculating the errors due to photon noise in the temperature, pressure, and number density profiles, making the usual assumptions necessary for the inversion of an occultation light curve. To accomplish this task we have recast the inversion equa-

0019-1035/78/0331-0186$02.00/0

tions into a simplified form, more appropriate for treating photon noise. Our analysis explicitly demonstrates the importance of the initial condition used for the inversion calculation, long recognized as critically influencing a large portion of the profiles. We describe a new procedure for establishing this initial condition and evaluating the uncertainty that it produces.

Assuming the basic validity of the inversion method, our final prescription for obtaining number density, pressure and temperature profiles, and their errors is directly applicable to light curves whose dominant photometric error is photon noise—such as the airborne observations of the ϵ Gem occultation (Elliot *et al.*, 1977b). For this class of light curves, the formulas developed here can be used to estimate, in advance of the occultation, the errors to be expected in temperature, pressure, and number density. For light curves containing significant amounts of other photometric noise, the errors calculated on the basis of our photon noise model are lower limits for the actual errors.

II. A NEW METHOD FOR INVERSION OF LIGHT CURVES

A. NOTATION AND ASSUMPTIONS

The occultation geometry for an immersion event is illustrated in Fig. 1. Starlight, incident from the left side of the figure, is refracted by a planetary atmosphere and received by a telescope a distance D from a spherical planet of radius R_p. As seen by the telescope, the apparent velocity of the occulted star perpendicular to the limb of the planet is $v_\perp$, and the starlight varies in intensity due to the process of differential refraction. A light ray whose unrefracted path makes the closet approach h to the center of the planet is refracted through an angle $\theta(h)$, which has a negative algebraic sign for the angles indicated in the figure. The x-axis lies parallel to the original direction of the light rays and coordinate r is the distance from the center of the planet. The atmosphere has a refractivity $\nu(r)$, the index of refraction minus unity. The shell notation of the figure will be defined later, when it is used for computations.

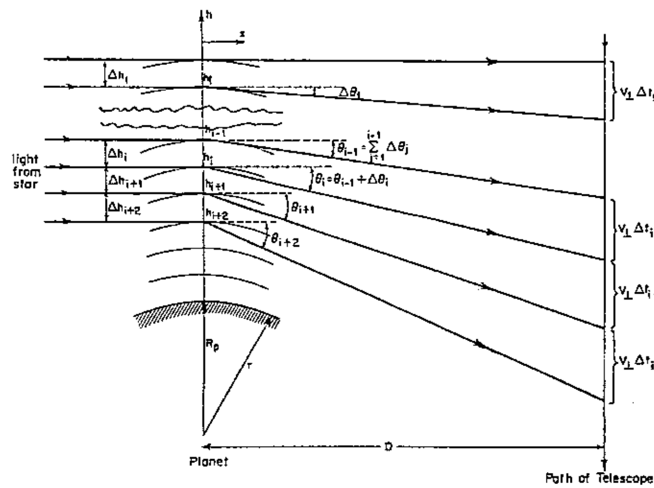

FIG. 1. Occultation geometry for an immersion event. Starlight is incident from the left and is received by a telescope a distance D from a spherical planet of radius R_p. As seen by the telescope, the starlight varies in intensity due to the process of differential refraction. Refer to the text for a complete description of notation.

To obtain the number density, pressure and temperature profiles of the planetary atmosphere from the occultation light curve, we make the following assumptions:

Atmosphere

(i) The approximate scale height H of the atmosphere satisfies the condition $H \ll R_p$.

(ii) The refractivity of the atmosphere $\nu(r)$ is a function of r only.

(iii) The atmosphere has uniform composition.

(iv) The atmosphere is in hydrostatic equilibrium.

(v) Rayleigh scattering and other forms of extinction are negligible when compared to the decrease in intensity due to differential refraction. This will be true if the distance D is large (Baum and Code, 1953).

Optics

(vi) The occulted star is a point source.

(vii) Diffraction effects are negligible (i.e., the ray optics approximation is used).

(viii) There is no ray-crossing (i.e., $d\theta(h)/dh < -1/D$; see Section V of Elliot and Veverka, 1976).

(ix) Bending angles are small (i.e., $|\theta| \ll 1$).

Noise

(x) The light curve received by the telescope contains photon noise.

B. Fundamental Equations

If $H/R_p \ll 1$, it can be shown that (Wasserman and Veverka, 1973)

$$\nu(h) = \frac{2}{\pi(2R_p)^{1/2}} \int_h^\infty (h'-h)^{1/2} d\theta(h'). \quad (1)$$

Then the number density $n(h)$ (cm^{-3}) is given by

$$n(h) = \mathfrak{L}\nu(h)/\nu_{STP}, \quad (2)$$

where $\mathfrak{L}$ is Loschmidt's number and ν_{STP} is the refractivity of the atmosphere at standard temperature and pressure for the wavelength of the observation. The pressure, $p(h)$, can be found by integrating the equation of hydrostatic equilibrium

$$dp(h) = -\bar{\mu} g n(h) dh/N_A, \quad (3)$$

where $\bar{\mu}$ is the mean molecular weight of the atmosphere and N_A is Avogadro's number. The gravitational acceleration g is assumed to be constant, but an altitude dependence could be included here if necessary. Integration of (3) yields

$$p(h) = \frac{4g\bar{\mu}\mathfrak{L}}{3\pi(2R_p)^{1/2}\nu_{STP}N_A} \times \int_h^\infty (h'-h)^{3/2} d\theta(h'). \quad (4)$$

Finally, the temperature $T(h)$ can be determined by combining (2), (4) and the perfect gas law:

$$T(h) = N_A p(h)/Rn(h), \quad (5)$$

where R is the universal gas constant.

The scale height $H(h) = RT(h)/\bar{\mu}g$ can be found from (5):

$$H(h) = \frac{2}{3} \int_h^\infty (h'-h)^{3/2} d\theta(h') \Big/ \int_h^\infty (h'-h)^{1/2} d\theta(h'). \quad (6)$$

We note that $H(h)$ is independent of the atmospheric composition. Since the scale height is the ratio of two differently weighted integrals of the same variable, much of the noise cancels out, and we shall find in Section III that a consequence of this is that temperature profiles can have smaller fractional errors than number density and pressure profiles.

To evaluate the integrals in (6), we will write them as summations. In Fig. 1 we have divided the atmosphere into shells of thickness Δh. For the ith shell we define the following quantities: h_i and h_{i-1}, the altitude of its lower and upper boundaries; $\Delta\theta(h_i)$, the increment in refraction angle for the $(i-1)$th and ith rays; Δt_i, the amount of time between the receipt of the $(i-1)$th and ith rays by the telescope; and ϕ_i, the average of the normalized stellar flux received by the telescope during the time interval Δt_i.

The function $\Delta\theta(h_i)$ can be found from the light curve flux $\phi(t)$ by a two-step process. Starting at a reference level h_{i-1}, we can find an implicit equation for the time Δt_i,

$$\Delta h = |h_i - h_{i-1}| = v_\perp \int_{t_{i-1}}^{t_{i-1}+\Delta t_i} \phi(t) dt. \quad (7)$$

After finding Δt_i from (7), we can now find the desired increment in refraction angle $\Delta\theta(h_i)$:

$$\Delta\theta(h_i) = \Delta h - v_\perp \Delta t_i/D \quad (8a)$$

$$= \left(\frac{-v_\perp}{D}\right) \int_{t_{i-1}}^{t_{i-1}+\Delta t_i} [1-\phi(t)] dt. \quad (8b)$$

C. Errors Caused by Photon Noise

The noise-free occultation flux $\phi(t)$ is not directly obtained from the observations, since photon noise (shot noise) is present in the light curve. Let the quantity $\epsilon^2(\phi)$ be the variance of the shot noise integrated for one second, computed from the Poisson statistics obeyed by photons. For a one second interval when $\phi(t)$ has a constant value ϕ, the average number of detected photons will be $\phi n_* + n_b$, where n_* and n_b are the rates of photons detected per second from the unocculted star and the background. (It is convenient to use units of seconds because the time scale for an occultation is $H/v_\perp$, which is typically of order one second.) For Poisson statistics the variance is equal to the mean, and after normalizing by n_*,

$$\epsilon(\phi) = (\phi n_* + n_b)^{1/2}/n_*. \quad (9)$$

The value of $\epsilon(\phi)$ for two limiting cases will be of interest later:

$$\epsilon(\phi) = (\phi/n_*)^{1/2} \quad \text{for } n_b = 0, \quad (10)$$

$$\epsilon(\phi) = n_b^{1/2}/n_* \quad \text{for } n_b \gg n_*. \quad (11)$$

Finally, the variance in the flux from the ith shell is given by

$$\sigma^2(\phi_i) = v_\perp \phi_i \epsilon^2(\phi_i)/\Delta h. \quad (12)$$

This equation is the fundamental relation for propagating errors from the light curve into number density, pressure, and temperature profiles. In this formulation, the fluxes $\{\phi_i\}$ are taken to be a set of independent random variables. All times $\{\Delta t_i\}$, defined by $\Delta h_i = v_\perp \phi_i \Delta t_i$, are taken to be known exactly, but there is an uncertainty in the location of the shell boundaries which correspond to known times on the light curve.

D. An Improved Initial Condition

There are two kinds of initial errors in the evaluation of the integrals in (1) and (4). First, there is truncation error, since in practice the limits of the integral must be finite. Second, the bending angle is so small at the onset of the occultation that noise fluctuations will completely dominate intensity variations due to the atmosphere. The first requires that the numerical inversion begin early enough to include all true variation, while the second indicates that starting too early will introduce additional errors. The problem we are left with can be stated as follows: Can we find an initial condition which utilizes all of the data in the light curve and which allows an accurate estimate of the errors due to random noise?

In previous work, three approaches have been used. The first is to begin the summation at some value for which $\phi_i \simeq 1$ and $\Delta\theta \approx 0$ (Wasserman and Veverka, 1973). The difficulty with this method is that an unnecessarily large error is introduced into the computation if the inversion is begun too soon, and information is lost if the inversion is begun too late. Additionally, as is shown in Section V, the results are sensitive to the starting point used. A second method has been to generate a sequence of $\Delta\theta_i$'s for the initial part of the light curve by assuming that the atmosphere is isothermal with the scale height determined from a least squares fit to the refractivity profile (Hubbard *et al.*, 1972). These $\Delta\theta_i$'s are then used to start the inversion until the flux has fallen to ~ 0.98. The objection to this approach has been that small uncertainties in the flux of the first point used in the inversion lead to large errors in estimated $\Delta\theta_i$. A final method has been to specify an initial temperature at an arbitrary altitude (Vapillon *et al.*, 1973).

We have developed an initial condition which utilizes an isothermal fit to the initial part of the light curve only. The procedure has the following features: (a) truncation errors are eliminated; (b) information further down on the light curve does not bias the initial isothermal fit; (c) the fit utilizes uncorrelated random variables whose errors can be determined directly; and (d) the arbitrary features of the other methods are avoided. The method assumes that the upper and lower baselines ($\phi = 1$ and 0 levels) have already been determined by some means.[1] First, $d\theta(h)/dh$ is determined from the data, using (7) and (8), between $h = h_{\max}$ and $h = h_0$. The altitude $h_{\max}$ corresponds to some point on the light curve which precedes the onset of the occultation, and h_0 corresponds to a point on the light curve where the flux has clearly diminished. The procedure used to determine h_0 is described below.

The function

$$\frac{d\theta}{dh}(h') = ca^{1/2}e^{-a(h'-h_0)} \tag{13}$$

is fit to the data in the least-squares sense. The form of (13) is chosen so that a and c are uncorrelated random variables whose errors, $\sigma(a)$ and $\sigma(c)$, can be determined from the fit. The scale height of the initial fit is given by $H_e = 1/a$, and $c = H_e^{1/2}d\theta(h_0)/dh$. Since the fit is performed on data which are equally spaced in altitude rather than in time, the formal errors in the fit have to be modified to account for the interpolation involved in converting data from the time to the space domain. If data are analyzed at very high time resolution, $\Delta\tau$, so that the condition $v_\perp\Delta\tau \ll \Delta h$ is satisfied, then many data points in time will be included in each Δh shell, and the effects of interpolation will be negligible. (In any case, we require $\Delta h \ll H$; there must be many shells per scale height in order for the numerical approximations to the integrals to be valid.) On the other hand, practical considerations often require $v_\perp\Delta\tau > \Delta h$ in order that $\Delta h \ll H$, and in this case it is important to correct the formal errors, $\sigma(a)_{\text{formal}}$ and $\sigma(c)_{\text{formal}}$. We have derived the following correction factor:

$$\sigma_{\text{true}} = \left(\frac{3}{2}\frac{v_\perp\Delta\tau}{\Delta h}\right)^{1/2}\sigma_{\text{formal}}. \tag{14}$$

In computing this factor, we have assumed that the initial fit is halted before $\phi \ll 1$. We emphasize that this correction is appropriate only if $v_\perp\Delta\tau > \Delta h$.

Finally, the value of h_0 is chosen so that the fitted scale height H_e is established with an error comparable to that associated with the inversion of later sections of the light curve. In practice this means experimenting with a range of h_0 and selecting the largest value for which $H_e(h_0)$ has settled down to a slowly varying function. With very noisy data, this point can be far down the light curve. Examples are discussed in Sections III and V.

[1] These can be estimated by fitting the Baum and Code equation to the light curve. Both the inversion scheme and the Baum and Code equation assume that all bending of rays by the planetary atmosphere is in the plane of Fig. 1. However, the lateral focussing effects of a spherical atmosphere can be important. For example, they are responsible for the formation of the central flash, a bright feature midway between immersion and emersion in the occultation of ϵ Gem by Mars (Elliot *et al.*, 1977b). It can be shown, however, that these effects can be neglected when determining baselines, as long as $H/R_p \ll 1$ (French, 1977). A briefer treatment is presented in Pannekoek (1904).

E. Number Density, Pressure, and Temperature Profiles and Their Associated Errors

We are now in a position to write the full expressions for $n(h)$, $p(h)$ and $H(h)$ and their associated errors. Let

$$I_m(h_i) = \int_{h_0}^{\infty} (h'-h_i)^m ca^{1/2}e^{-a(h'-h_0)}dh' \tag{15}$$

and

$$\Sigma_m(h_i) = \frac{1}{1+m}(\Delta h)^m \sum_{j=j\min+1}^{i} \Delta\theta_j \times[(i-j)^{m+1} - (i-j+1)^{m+1}], \tag{16}$$

where $j_{\min}$ is the index of the shell between $h = h_0$ and $h = h_0 + \Delta h$. In (16), we have preintegrated the factor $(h' - h_i)^m$. Expressed in terms of the set of independent variables $\{\phi_i\}$, (16) can be written as

$$\Sigma_m(h_i) = \frac{1}{D(1+m)}\sum_{j=j\min+1}^{i}\left(\frac{1-\phi_j}{\phi_j}\right) \times\Big[\Big(\sum_{k=j}^{i} v_\perp\phi_k\Delta t_k\Big)^{m+1} - \Big(\sum_{k=j+1}^{i} v_\perp\phi_k\Delta t_k\Big)^{m+1}\Big]. \tag{17}$$

The random error associated with $\Sigma_m(h_i)$ is

$$\sigma^2[\Sigma_m(h_i)] = \sum_{j=j\min+1}^{i}\left[\frac{\partial\Sigma_m(h_i)}{\partial\phi_j}\right]^2\sigma^2(\phi_j) \tag{18}$$

and the variance of $I_m(h_i)$ is

$$\sigma^2[I_m(h_i)] = [\partial I_m(h_i)/\partial a]^2\sigma^2(a) + [\partial I_m(h_i)/\partial c]^2\sigma^2(c). \tag{19}$$

The number density in the ith shell is given by

$$n(h_i) = \frac{2\mathcal{L}}{\pi(2R_p)^{1/2}\nu_{\text{STP}}} \times[I_{1/2}(h_i) + \Sigma_{1/2}(h_i)]. \tag{20}$$

The fractional error in $n(h_i)$ is

$$\frac{\sigma[n(h_i)]}{n(h_i)} = \frac{\{\sigma^2[I_{1/2}(h_i)] + \sigma^2[\Sigma_{1/2}(h_i)]\}^{1/2}}{I_{1/2}(h_i) + \Sigma_{1/2}(h_i)}. \tag{21}$$

Similarly,

$$p(h_i) = \frac{4g\bar{\mu}\mathcal{L}}{3\pi(2R_p)^{1/2}\nu_{\text{STP}}N_A} \times[I_{3/2}(h_i) + \Sigma_{3/2}(h_i)], \tag{22}$$

$$\frac{\sigma[p(h_i)]}{p(h_i)} = \frac{\{\sigma^2[I_{3/2}(h_i)] + \sigma^2[\Sigma_{3/2}(h_i)]\}^{1/2}}{I_{3/2}(h_i) + \Sigma_{3/2}(h_i)}, \tag{23}$$

$$H(h_i) = \frac{2}{3}\frac{[I_{3/2}(h_i) + \Sigma_{3/2}(h_i)]}{[I_{1/2}(h_i) + \Sigma_{1/2}(h_i)]}, \tag{24}$$

$$\sigma^2[H(h_i)] = \left(\frac{\partial H}{\partial a}(h_i)\right)^2\sigma^2(a) + \left(\frac{\partial H}{\partial c}(h_i)\right)^2\sigma^2(c) + \sum_{j=j\min+1}^{i}\left(\frac{\partial H(h_i)}{\partial(\phi_j)}\right)^2\sigma^2(\phi_j). \tag{25}$$

Finally the error in the altitude difference $(h_j - h_i)$ is given by

$$\sigma^2(h_j - h_i) = \sum_{k=j+1}^{i}(\Delta h/\phi_k)^2\sigma^2(\phi_k). \tag{26}$$

The evaluation of these quantities is described in Appendix A.

III. THE NATURE OF THE ERRORS

In order to gain insight into the nature of fractional errors in number density, pressure, and scale height, we have obtained solutions to (21), (23), and (25) for the special case of an isothermal atmosphere with a known noise level. (We stress that these equations are valid for *any* atmosphere which satisfies the assumptions in Section IIA.) Since $\epsilon(\phi)$ is a function of both background and stellar fluxes [Eqn. (9)], we have treated two limiting cases: background flux much greater than stellar flux, $n_b \gg n_*$; and background flux much less than stellar flux throughout the light curve, or, in the limit, $n_b = 0$.

Figure 2 illustrates our results for the case $(v_\perp/H)^{1/2}\epsilon(\phi) = 0.01$, where $\epsilon(\phi)$ is evaluated at $\phi = 1.0$. Fractional errors in number density, pressure, scale height, $\Delta\theta$, and the error in altitude difference $(h_0 - h)/H$ (E_n, E_p, E_H, $E_{\Delta\theta}$, and E_h, respectively) are shown as a function of depth in the atmosphere and of normalized flux of the light curve. $E_{\Delta\theta}$ has been computed for the case $(v_\perp/\Delta h)^{1/2}\epsilon(\phi) = 0.01$. Note that, in this figure, the light curve is plotted against depth in the atmosphere, rather than against time. The upper branch of each curve corresponds to the case, $n_b \gg n_*$, and the lower branch to the case, $n_b = 0$.

The fractional errors in Fig. 2 are computed using the results of Appendix A, without utilizing an initial fit to the data and assuming that the inversion was begun five scale heights above half-light. We determined the point h_0 in (15) at which the scale height error in the initial fit is equal to the scale height error, $\sigma[H(h_0)]$ for the case shown. This occurs at $\phi = 0.60$ and $h_0 = 0.41H$, for an isothermal atmosphere. If the initial fit is extended to a deeper level (smaller h_0), the fractional errors will be smaller than those shown in Fig. 2; if h_0 is larger than $0.41H$, the fractional errors in Fig. 2 will be slight underestimates for the first scale height or so below h_0. The choice of h_0 in a practical case is discussed in Section V.

Figure 2 can be best understood by examining the nature of the error in $\Sigma_m(h_i)$. In (16) there is an uncertainty in $\{\Delta\theta_j\}$ and also in $(h_j - h_i)^m$, which has been preintegrated in this equation. From (7), (8), and (12) we find

$$\frac{\sigma(\Delta\theta_i)}{\Delta\theta_i} = \left(\frac{v_\perp\phi_i}{\Delta h}\right)^{1/2} \frac{\epsilon(\phi_i)}{(1-\phi_i)}. \quad (27)$$

Equation (27) illustrates that $\sigma(\Delta\theta)/\Delta\theta$ is largest near $\phi = 1$, when noise causes much more variation in apparent flux than does the slight bending due to the atmosphere. As ϕ approaches zero, so does the fractional error in $\Delta\theta$. This is shown in Fig. 2 as $E_{\Delta\theta}$.

Equation (26) gives

$$\frac{\sigma(h_j - h_i)}{H} = \frac{(v_\perp\Delta h)^{1/2}}{H}\left[\sum_{k=j+1}^{i} \frac{\epsilon^2(\phi_k)}{\phi_k}\right]^{1/2}. \quad (28)$$

This is shown in Fig. 2 as E_h, with h_j taken as $5H$. For constant $\epsilon(\phi)$, E_h increases rapidly as $\phi \to 0$, and this is reflected in the corresponding increase in E_n, E_p, and E_H. For $n_b = 0$, $\epsilon(\phi)$ is proportional to $\phi^{1/2}$ [see Eq. (10)], and as $\phi \to 0$, E_n, E_p, and E_H approach constant limiting values.

From the form of (1), (4), and (6), it is evident that the deduced values of $n(h)$, $p(h)$, and $H(h)$ depend on the nature of the entire light curve prior to that point. This reflects the simple fact that a grazing ray at altitude h is refracted not only by the atmosphere at h, but also by the atmosphere along the rest of its path. We can see the manner in which the prior data are weighted by plotting the integrands of (15) with $m = \frac{3}{2}$ and $m = \frac{1}{2}$, for the case of an isothermal atmosphere. These are used in determining $p(h)$ and $n(h)$, whose ratio is proportional to the scale height. The integrands are shown in Fig. 3, where the curves have been normalized to unity at their maxima, and where altitude, z, is measured in scale heights above h. The main contribution to the integral for $n(h)$

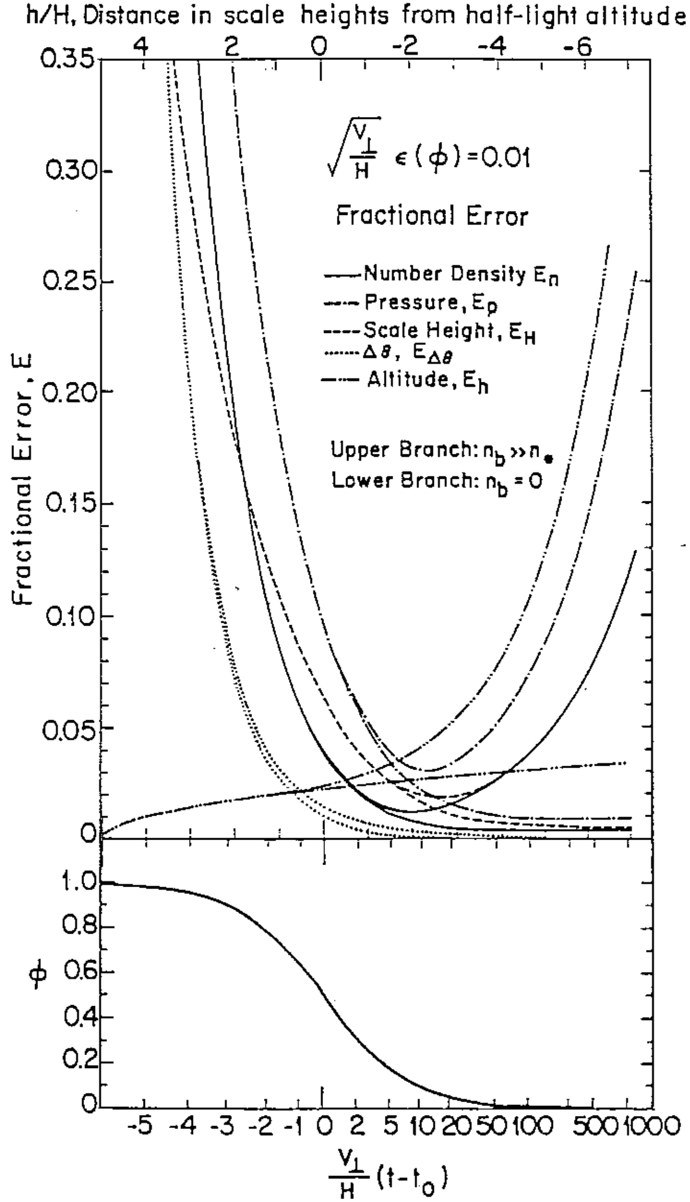

FIG. 2. Fractional errors in $n(h)$, $p(h)$, $H(h)$, $\Delta\theta(h)$, and altitude $(h_0 - h)/H$, computed for an isothermal atmosphere. E_n, E_p, E_H, and E_h were determined for the case $(v_\perp/H)^{1/2}\epsilon(\phi) = 0.01$, and $h_0 = 5H$, and $E_{\Delta\theta}$ for the case $(v_\perp/\Delta h)^{1/2}\epsilon(\phi) = 0.01$, where $\epsilon(\phi)$ is evaluated at $\phi = 1$. The upper branches correspond to the limit of background flux much greater than stellar flux, $n_b \gg n_*$, and the lower branches to the case, $n_b = 0$. The light curve, below, allows fractional errors at different altitudes to be related to normalized flux, ϕ, and time from half-light, t, along the light curve.

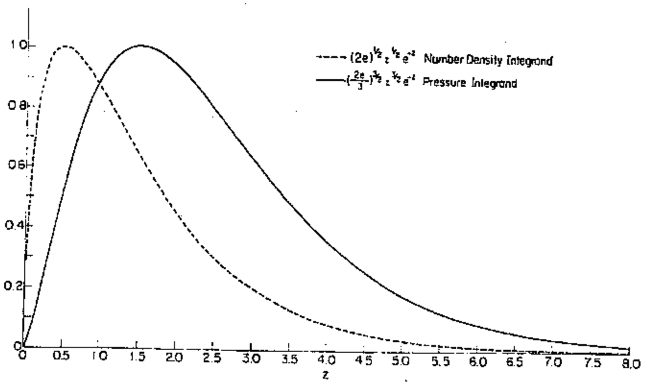

FIG. 3. Integrands used in the computation of $n(h)$ and $p(h)$, for an isothermal atmosphere. The abscissa, z, is the altitude in the atmosphere (measured in scale heights) above the altitude h at which number density and pressure are to be computed. The curves, normalized to unity at their maxima, show how the computed values of $n(h)$ and $p(h)$ depend upon a knowledge of the atmospheric structure for several scale heights above h. In computing $n(h)$, the most significant contribution comes from an altitude range, h to $h + 2.5H$, while for $p(h)$, the main contribution comes from an altitude range $h + 0.5H$ to $h + 4.5H$. This strong weighting of prior data is responsible for the characteristics of the fractional errors, shown in Fig. 2.

comes from a fairly narrow altitude range centered at about $h + 0.5H$, while the main contribution to the integral for $p(h)$ is centered at $h + 1.5H$, with significant contribution from as high as $h + 4.5H$. In other words, the data used to determine $n(h)$ are, in a sense, more "local" than those for $p(h)$.

The fractional errors in $n(h)$ and $p(h)$ are determined from similar weighted averages of the errors in $(h_j - h_i)^m$ and $\Delta\theta$ of prior data. As the inversion proceeds, E_n decreases rapidly because it weights a fairly narrow range of prior data whose fractional errors in $\Delta\theta$ are decreasing rapidly; E_p minimizes somewhat later because it weights most strongly a range of prior data at higher altitude, whose fractional errors in $\Delta\theta$ are still large. In this region the error in $(h_j - h_i)^m$ does not contribute strongly. If $n_b = 0$, the fractional errors E_n, E_p, and E_H will decrease as the inversion is continued, because $E_{\Delta\theta} \to 0$ and E_h is rising only slowly. If $n_b \gg n_*$, E_p rises from its minimum rapidly, in response to the rapid rise in E_h; E_n and E_H rise more slowly because of their weaker dependence on errors in $(h_j - h_i)$.

It is important to note that E_H is comparable to E_n and E_p; as long as all of the assumptions of the method are satisfied, temperature profiles are as accurate as number density and pressure profiles. Additionally, the flux level corresponding to minimum errors is low, due to the weighting functions of Fig. 3. Even for the case $n_b \gg n_*$, the fractional error in H does not rise to double its minimum value until $\phi = 0.001$, $h/H = -4.6$, and $v_\perp(t - t_0)H = 103$. The lesson is that inversions may be continued to deeper levels than previously suspected before errors due to photon noise become large. Inverting in shells of Δh rather than Δt is advantageous in this context because the inversion need not be terminated at the first point at which the apparent flux is negative. Ultimately, uncertainty in the lower baseline will be a more important source of error than photon noise.

IV. THE QUALITY OF AN OCCULTATION: EFFECTS OF SHOT NOISE

It is useful to have a simple way to predict the quality of an occultation from the fundamental quantities $v_\perp$, H, ϕ, and $\epsilon(\phi)$. The calculations of fractional errors for an isothermal atmosphere, described above, can serve as a guide to the magnitude of the minimum errors we can expect. Expected fractional errors can be obtained by scaling the solutions for E_n, E_p, E_H, $E_{\Delta\theta}$, and E_h in Fig. 2 according to the relations

$$\left.\begin{aligned} &\frac{\sigma[n(h)]}{n(h)} \\ &\frac{\sigma[p(h)]}{p(h)} \\ &\frac{\sigma[H(h)]}{H(h)} \\ &\frac{\sigma(5H-h)}{H} \end{aligned}\right\} = \frac{\epsilon(1.0)}{0.01}\left(\frac{v_\perp}{H}\right)^{1/2} \begin{cases} E_n(h), & (29) \\ E_p(h), & (30) \\ E_H(h), & (31) \\ E_h(h), & (32) \end{cases}$$

$$\frac{\sigma(\Delta\theta)(h)}{\Delta\theta(h)} = \frac{\epsilon(1.0)}{0.01}\left(\frac{v_\perp}{\Delta h}\right)^{1/2} E_{\Delta\theta}(h). \tag{33}$$

For the case $n_b \gg n_*$, the upper branch solutions in Fig. 2 should be used. If $n_b = 0$, the lower branch solutions are appropriate. In (29)–(33), $\epsilon(\phi)$ has been evaluated at $\phi = 1.0$.

Expected minimum fractional errors and the flux levels at which they occur are:

$n_b \gg n_*$:

$$\left.\begin{aligned} &\left.\frac{\sigma[n(h)]}{n(h)}\right|_{\min} \\ &\left.\frac{\sigma[p(h)]}{p(h)}\right|_{\min} \\ &\left.\frac{\sigma[H(h)]}{H(h)}\right|_{\min} \end{aligned}\right\} = \left(\frac{v_\perp}{H}\right)^{1/2} \epsilon(1.0) \begin{cases} 1.21\ (\phi = 0.13), & (34) \\ 3.05\ (\phi = 0.09), & (35) \\ 1.96\ (\phi = 0.07), & (36) \end{cases}$$

$n_b = 0$:

$$\left.\begin{aligned} &\left.\frac{\sigma[n(h)]}{n(h)}\right|_{\min} \\ &\left.\frac{\sigma[p(h)]}{p(h)}\right|_{\min} \\ &\left.\frac{\sigma[H(h)]}{H(h)}\right|_{\min} \end{aligned}\right\} = \left(\frac{v_\perp}{H}\right)^{1/2} \epsilon(1.0) \begin{cases} \le 0.42 & (37) \\ \le 0.93, & (38) \\ \le 0.56. & (39) \end{cases}$$

TABLE I

Photon Noise Errors for Occultations

Occultation	$(v_1/H)^{1/2}\epsilon(\phi)^a$	$\sigma(H)/H\|_{min}$	Comments
β Scorpii by Jupiter[b]	0.0004 0.0002	0.0007	Other noise sources definitely more important than shot noise in determining minimum errors
ϵ Geminorum by Mars[c]	0.012 0.007	0.023	Errors due to photon noise consistent with mutual agreement of temperature profiles
SAO 158687 by Uranus[d]	0.003 0.0017	0.006	

[a] Evaluated for $\phi = \frac{1}{3}$. Lower # at $\phi = 1$.
[b] 154-cm telescope, $\lambda_0 = 3530$ Å, $\Delta\lambda = 400$ Å (Veverka *et al.*, 1974).
[c] 91-cm telescope, $\lambda_0 = 4500$ Å, $\Delta\lambda = 100$ Å (Elliot *et al.*, 1977b).
[d] 91-cm telescope, $\lambda_0 = 8000$ Å, $\Delta\lambda = 300$ Å (Elliot *et al.*, 1977a).

In (37)–(39), the inequality signs indicate that, for $n_b = 0$, the fractional errors had not reached their limiting values before $\phi = 0.001$, the point at which calculations were stopped. This is evident in Fig. 2.

As an example of the use of these equations, we have estimated the minimum fractional errors in scale height due to shot noise for several occultations. The results are given in Table I. It should be recognized that $\epsilon(\phi)$ is not an intrinsic property of a particular occultation, and its value will depend on how the occultation is observed. For example, the telescope aperture and filter bandwidth are important factors.

V. APPLICATION OF THE INVERSION METHOD: AN EXAMPLE

To illustrate several important features of the new inversion method, we have utilized the equations developed in Section II to invert an isothermal light curve with added random noise. For this case we let $H = 10$ km, $v_1 = 10$ km sec^{-1}, $\epsilon(\phi) = 0.02$, and $\Delta h = 1$ km. These parameters give a noise factor of $(v_1/H)^{1/2}\epsilon(\phi) = 0.02$, comparable to that of the airborne observations of the occultation of ϵ Gem by Mars. We assumed that $n_b \gg n_*$, so that $\epsilon(\phi)$ can be regarded as constant throughout the occultation [see Eq. (11)]. The light curve is shown in Fig. 4. The solid line is a noise-free isothermal light curve computed from the well-known equation of Baum and Code (1953).

Two methods of numerical inversion were used to deduce the scale height. The first utilizes the full theory developed above, together with the new initial condition, an isothermal fit to the initial data in the light curve. The second method does not utilize the new initial condition, and in effect assumes that $H = 0$ at the onset of the inversion.

Figure 5 presents the results of the inversions. For the case shown on the left, an isothermal fit to the initial data, using (13), gave $H_c = 10.88$ km $\pm$ 1.59. The region of the light curve used in the fit is shown in Fig. 4, and begins six scale heights above half-light, and ends at $\phi \approx 0.60$. The error bars on the temperature profile were computed from (25), and have a total length of two standard deviations. At all altitudes, the error bars are consistent with the actual scale height of 10 km. Errors in altitude are not shown, but they can be estimated from Fig. 2. The characteristics of E_H in Fig. 2 are reflected in the errors of the temperature profile: the errors are initially very large, and eventually minimize at about three scale heights below the half-light level, after which they rise slowly. An additional 56 sec of data would have had to be included in the inversion before the deduced temperature profile

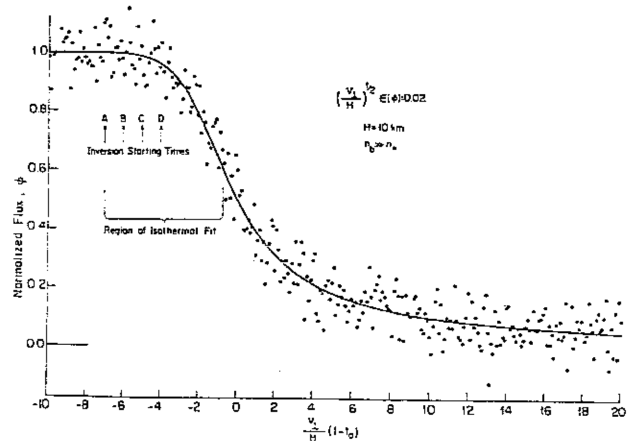

FIG. 4. Isothermal light curve with scale height $H = 10$ km and noise figure $(v_1/H)^{1/2}\epsilon(\phi) = 0.02$; it is assumed that $n_b \gg n_*$. The solid line is the noise-free light curve. The results of inversion of the noisy light curve are shown in Fig. 5. The inversion was terminated at $v_1(t - t_0)/H = 35.0$, although the curve is shown above only to $v_1(t - t_0)/H = 20.0$.

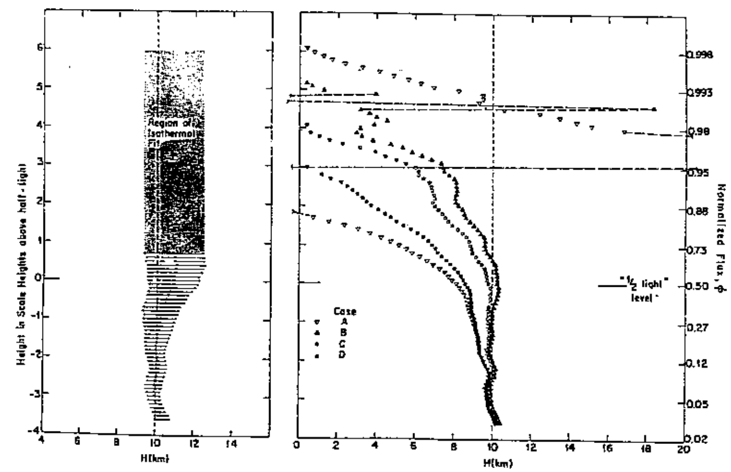

FIG. 5. Scale height profiles obtained from inversion of the light curve shown in Fig. 4. The true scale height is 10 km. The profile at the left was obtained using the new method described in this paper. The error bars are consistent with the true scale height. Errors in altitude are not shown, but the one standard deviation values are about ± 0.5 km at the half-light altitude and ± 1.5 km at the lower end of profile. On the right, profiles were obtained by assuming $H = 0$ at the onset of the inversion. The inversion starting times used for Cases A, B, C, and D are shown in Fig. 4, along with the region of the light curve used in the initial fit.

could be extended a scale height deeper in the atmosphere. At that depth, for the parameters of this example, it can be seen from Fig. 2 that $\sigma(H)/H$ would have increased only to 0.075.

It is important to recognize that the noise in successive points is correlated. For this reason, adjacent points agree better than implied by the error bars. In other words, the error bars refer to the gross positioning of the profile, rather than to the much smaller uncertainties in local temperature variations.

On the right of Fig. 5, we show the results of inversion of the same light curve, but without utilizing an isothermal fit to the initial data. The inversions were begun at four different starting times, corresponding to six, five, four, and three scale heights above half-light; see Fig. 4 for the corresponding positions on the light curve. Case A, the inversion utilizing the most data, converges most slowly to the correct scale height, H, illustrating that errors tend to diverge as the inversion is begun earlier and earlier. Cases B and C give results comparable to the inversion utilizing the initial fit. Case D illustrates the problem of beginning the inversion too late. Although the flux has dropped only to $\phi = 0.95$ at the onset of the inversion, the temperature profile does not converge to within 10% of the actual scale height until $\phi = 0.30$.

We have obtained four substantially different temperature profiles from the same initial data, by changing only the starting point of the inversion and assuming that $H = 0$ initially. Lacking *a priori* knowledge of the true temperature profile, there would be no clear best choice among the curves. In contrast, the new inversion method is less sensitive to the starting time, does not assume a zero temperature at the onset of inversion, and provides a quantitative measure of the error at all altitudes due to a known source of noise.

An important consideration in the use of the new method is the choice of how much of the light curve should be included in the initial isothermal fit. In the parlance of (15), what governs the choice of h_0? If only the first part of the curve is used, (27) shows that the data are noise dominated, and the errors in the fit $[\sigma(a)$ and $\sigma(c)]$ will be enormous; they will propagate down through the entire light curve, as seen in (25). On the other hand, if too much of the light curve is used in the initial fit, information about detailed temperature variation will be masked. Additionally, errors in a and c may actually grow as more data are fit, because the assumption that the atmosphere is isothermal may become less realistic. The method may be unreliable if the isothermal approximation is strongly violated.

Although we have found that, for an isothermal atmosphere, it is optimum to fit to the $\phi = 0.60$ level, this can only serve as a rough guide in actual practice, because there is no guarantee that the sampled atmosphere is isothermal. Our strategy is to fit successively larger sections of the data until the deduced scale height, H_c, is insensitive to changes in h_0 which are small compared to H_c. In Table II, we give the results of a variety of fits to the initial data in this example to show the change in H_c as the region of the fit is varied. By this means, the initial fit serves the function of damping the erratic initial behavior of the inversion and of rendering the inversion insensitive to its starting point. It provides an estimate of errors due to photon noise, and by stopping the fit as early as possible, the atmospheric temperature profile can be determined by the inversion over a significant altitude range.

TABLE II

VARIATION OF H_c WITH RANGE OF DATA USED FOR FIT

h_{max}/H	h_0/H	$\phi(h_0)$	H_c (km)[a]
6.0	1.1	0.75	11.98 ± 2.83
	0.6	0.65	10.88 ± 1.59
5.0	2.5	0.92	10.08 ± 8.56
	2.4	0.92	8.52 ± 5.79
4.0	2.0	0.88	7.73 ± 2.93
	1.4	0.80	13.35 ± 4.10
	0.9	0.71	9.67 ± 1.58
	0.3	0.57	12.31 ± 1.51
3.0	1.0	0.73	12.35 ± 2.80
	0.4	0.60	12.71 ± 1.99

[a] True value of scale height = 10 km.

VI. DISCUSSION

We have used the new inversion method to obtain number density, pressure, and temperature profiles of the Martian atmosphere from airborne observations of the occultation of ϵ Gem on 8 April 1976 (Elliot *et al.*, 1977b). Three light curves were obtained simultaneously, each probing the same region of the Martian atmosphere, but each containing a different sample of photon noise. Hence the profiles obtained from different light curves should agree within their error bars—which they do—providing an internal consistency check of our method for computing errors.

Further analysis of the temperature profiles obtained from the ϵ Gem occultation showed that temperature variations, having a vertical scale of order one scale height, are determined much more precisely than the mean temperature, in the presence of photon noise (see Figs. 12 and 13 in Elliot *et al.*, 1977b). The present analysis could be extended to understand quantitatively the reliability of temperature information over various length scales, perhaps by a power spectrum analysis of temperature variations.

Fractional errors in $n(h)$, $p(h)$, and $H(h)$ due to photon noise minimize at very low fluxes, and at this point other sources of uncertainty become important. Baseline instability and uncertainty remain to be studied in detail. Additionally, as the inversion is extended into the noise-dominated tail of a light curve, statistical fluctuations will give solutions Δt_i in (7) even if the flux from the star is zero. This would have the effect of producing a spurious high-temperature tail on the deduced profile. In practice, inversions must be terminated for other reasons before this effect becomes important.

To some extent, each of the assumptions in Section IIA is only approximately satisfied. On the basis of scintillation theory, several authors (Young, 1976; Jokipii and Hubbard, 1977) have concluded that the assumption of spherical symmetry is so strongly violated as to invalidate the inversion method. By comparing the light curves obtained by several observers of the ϵ Gem occultation, it may be possible to place some limits on the degree of spherical symmetry of the Martian atmosphere, and hence to test this important assumption. This work is being pursued.

VII. CONCLUSIONS

With the new method of analysis of occultation light curves described above, we are able to place error bars on temperature, pressure, and number density profiles due to photon noise in the data, given the assumptions stated in Section IIA. An improved initial condition renders the inversion less sensitive to its starting point, and thus is less arbitrary than previous methods. An important result is that temperature profiles are shown to be as reliable as refractivity, number density, and pressure profiles. The manner in which prior data are weighted is responsible for large initial fractional errors in $n(h)$, $p(h)$, and $H(h)$, but also accounts for the fact that errors in these quantities due to photon noise minimize at very low flux levels. Consequently, as long as baselines are stable, the inversion can be extended deep in the atmosphere; by inverting in increments Δh, rather than Δt, the inversion need not be halted when the first negative data point is reached.

We have computed the errors in $n(h)$, $p(h)$, and $H(h)$ for an isothermal light curve with a known level of photon noise. The noise quality of an occultation can be estimated by scaling the isothermal solution to the appropriate value of $(v_\perp/H)^{1/2}\epsilon(\phi)$. Fractional errors due to photon noise are only a few percent when $(v_\perp/H)^{1/2}\epsilon(\phi) \approx 0.01$, a reasonable value for high quality observations. Additionally, we have shown that minimum fractional errors in scale height determined from the inversion are comparable to those from an isothermal fit to a noisy isothermal light curve.

APPENDIX A

We derive here the quantities used to determine $\sigma^2[\Sigma_m(h_i)]$, $\sigma^2[H(h_i)]$, and $\sigma^2[I_m(h_i)]$ given in Section IIE. From (18),

$$\sigma^2[\Sigma_m(h_i)] = \sum_{j=j\min+1}^{i}\left[\frac{\partial\Sigma_m(h_i)}{\partial\phi_j}\right]^2\sigma^2(\phi_j). \quad (A1)$$

The variance in ϕ_j, $\sigma^2(\phi_j)$ is given by (12). Let

$$\Gamma_j = \frac{(1-\phi_j)}{(1+m)D\phi_j}\Big[\Big(\sum_{l=j}^{i} v_\perp\phi_l\Delta t_l\Big)^{m+1} - \Big(\sum_{l=j+1}^{i} v_\perp\phi_l\Delta t_l\Big)^{m+1}\Big]. \quad (A2)$$

Then

$$\Sigma_m(h_i) = \sum_{j=j\min+1}^{i}\Gamma_j \quad (A3)$$

and

$$\frac{\partial\Sigma_m}{\partial\phi_j} = \frac{\partial\Gamma_j}{\partial\phi_j} + \sum_{k=j\min+1}^{j-1}\frac{\partial\Gamma_k}{\partial\phi_j}. \quad (A4)$$

From (A2) and the relation $\Delta h = v_\perp\phi_j\Delta t_j$, we find

$$\frac{\partial\Gamma_j}{\partial\phi_j} = \frac{-\Delta h^{m+1}}{D(1+m)\phi_j^2}[(1+m)(\phi_j-1)(i-j+1)^m + (i-j+1)^{m+1} - (i-j)^{m+1}] \quad (A5)$$

and

$$\left.\frac{\partial\Gamma_k}{\partial\phi_j}\right|_{k\neq j} = \frac{\Delta h^{m+1}}{D\phi_j\phi_k}(1-\phi_k) \times[(i-k+1)^m - (i-k)^m] \quad (A6)$$

All of the terms in (A1) are now known.

From (25),

$$\sigma^2[H(h_i)] = \left(\frac{\partial H(h_i)}{\partial a}\right)^2\sigma^2(a) + \left(\frac{\partial H(h_i)}{\partial c}\right)^2\sigma^2(c) + \sum_{j=j\min+1}^{i}\left(\frac{\partial H(h_i)}{\partial\phi_j}\right)^2\sigma^2(\phi_j). \quad (A7)$$

The variances in a and c are determined from the fit of (13) to the data as modified by (14). The partial derivatives in (A7) are:

$$\frac{\partial H(h_i)}{\partial a} = \frac{\frac{2}{3}\frac{\partial I_{3/2}(h_i)}{\partial a} - H(h_i)\frac{\partial I_{1/2}(h_i)}{\partial a}}{[I_{1/2}(h_i)+\Sigma_{1/2}(h_i)]}, \quad (A8)$$

$$\frac{\partial H(h_i)}{\partial c} = \frac{\frac{2}{3}\frac{\partial I_{3/2}(h_i)}{\partial c} - H(h_i)\frac{\partial I_{1/2}(h_i)}{\partial c}}{[I_{1/2}(h_i)+\Sigma_{1/2}(h_i)]}, \quad (A9)$$

$$\frac{\partial H(h_i)}{\partial\phi_j} = \frac{\frac{2}{3}\frac{\partial\Sigma_{3/2}(h_i)}{\partial\phi_j} - H(h_i)\frac{\partial\Sigma_{1/2}(h_i)}{\partial\phi_j}}{[I_{1/2}(h_i)+\Sigma_{1/2}(h_i)]}, \quad (A10)$$

where the derivatives in Σ_m have been defined in (A4)–(A6). Letting $u = a(h_0 - h_i)$, we find from (15)

$$\partial I_m(h_i)/\partial a = [(u+\tfrac{1}{2})/a]I_m(h_i) - I_{m+1}(h_i), \quad (A11)$$

$$\partial I_m(h_i)/\partial c = I_m(h_i)/c, \quad (A12)$$

where

$$I_{1/2}(h) = (c/a)[u^{1/2} + \tfrac{1}{2}\pi^{1/2}e^u \operatorname{erfc}(u^{1/2})], \quad (A13)$$

$$I_{3/2}(h) = (c/a^2)[u^{1/2}(u+\tfrac{3}{2}) + \tfrac{3}{4}\pi^{1/2}e^u \operatorname{erfc}(u^{1/2})], \quad (A14)$$

$$I_{5/2}(h) = (c/a^3)\left[u^{1/2}\left(u^2+\frac{5}{2}u+\frac{15}{4}\right) + \frac{15}{8}(\pi)^{1/2}e^u \operatorname{erfc}(u^{1/2})\right], \quad (A15)$$

and

$$\operatorname{erfc}(x) = \left(\frac{2}{\pi^{1/2}}\right)\int_x^\infty e^{-t^2}dt. \quad (A16)$$

The fractional error in H can be computed from (A7).

APPENDIX B

Isothermal curve fitting has often been used to obtain an estimate of the mean scale height of the atmosphere sampled by the light curve. The merits and hazards of this practice have been the subject of considerable debate, and we wish to show only that, for the high background case ($n_b \gg n_*$), the error in an isothermal fit to a noisy isothermal light curve is approximately equivalent to the minimum error given by the inversion method. In other words, even in the most favorable case for an isothermal fit, its error is not significantly smaller than that given by the inversion method.

Assume that the isothermal light curve equation of Baum and Code, Eq. (B1), is being fit to an isothermal light curve with known noise $\epsilon(\phi)$, but unknown scale height, H, and midtime, t_0. We assume that the baselines are known exactly.

$$v_\perp(t-t_0)/H = (1/\phi - 2) + \ln(1/\phi - 1). \quad (B1)$$

Then the errors in the values of H and t_0 given by the fit can be computed from standard formulas (Clifford, 1973):

$$\sigma(H) = (c_{t_0}/d)^{1/2}, \quad (B2)$$

$$\sigma(t_0) = (c_H/d)^{1/2}, \quad (B3)$$

where

$$d = c_H c_{t_0} - c^2_{Ht_0}, \quad (B4)$$

$$c_{t_0} = [1/\epsilon^2(\phi)]\int_{-\infty}^{\infty}(\partial\phi/\partial t_0)^2 dt, \quad (B5)$$

$$c_H = [1/\epsilon^2(\phi)]\int_{-\infty}^{\infty}(\partial\phi/\partial H)^2 dt, \quad (B6)$$

$$c_{Ht_0} = [1/\epsilon^2(\phi)]\int_{-\infty}^{\infty}(\partial\phi/\partial H)(\partial\phi/\partial t_0)dt. \quad (B7)$$

The correlation coefficient for H and t_0 is

$$\rho(H, t_0) = -c_{Ht_0}/(c_H c_{t_0})^{1/2}. \quad (B8)$$

Evaluating the above expressions after some manipulation, we find

$$c_{t_0} = [v_\perp/(\epsilon^2(\phi)H)]\int_0^1 \phi^2(1-\phi)d\phi = v_\perp/12H\epsilon^2(\phi), \quad (B9)$$

$$c_H = [1/v_\perp H\epsilon^2(\phi)]\int_0^1[(1/\phi - 2) + \ln(1/\phi - 1)]^2\phi^2(1-\phi)d\phi \approx 0.441/v_\perp H\epsilon^2(\phi), \quad (B10)$$

$$c_{Ht_0} = [1/H\epsilon^2(\phi)]\int_0^1[(1/\phi - 2) + \ln(1/\phi - 1)]\phi^2(1-\phi)d\phi = -1/24H\epsilon^2(\phi), \quad (B11)$$

$$d = 0.035/H^2\epsilon^4(\phi). \quad (B12)$$

From the above quantities, we find the fractional error in scale height obtained from an isothermal fit to the entire light curve to be

$$\sigma(H)/H = 1.54(v_\perp/H)^{1/2}\epsilon(\phi). \quad (B13)$$

By comparison, the minimum fractional error in scale height given by the inversion method for the same conditions is given from Section IV as

$$\sigma(H)/H|_{\min} = 1.96(v_\perp/H)^{1/2}\epsilon(\phi). \quad (B14)$$

We conclude that the inversion method has minimum fractional errors comparable to those of an isothermal fit for the case of a noisy isothermal light curve.

The error in the estimate to the midtime, t_0, from the isothermal fit, is

$$\sigma(t_0) = 3.55(H/v_1)^{1/2}\epsilon(\phi). \quad \text{(B15)}$$

This gives a fundamental limit to the accuracy of the "half-light" time, a quantity which is useful for occultation astronomy (Taylor, 1976).

Finally, the correlation coefficient has the value $\rho_{Ht_0} = 0.217$. This very low value means that the formal error in t_0 will be nearly the same whether or not H is a free parameter in the fit, and vice versa.

ACKNOWLEDGMENTS

We wish to thank L. H. Wasserman for very helpful discussions concerning an earlier version of this paper, and acknowledge several helpful suggestions from J. T. Jokipii and D. M. Hunten as referees of this paper. Additionally, we are grateful to M. Roth for help in preparing the manuscript and B. Boettcher for drawing the figures. This work was supported in part by NASA Grants NGL 33-010-086, NSG-7126, and NSG-2174. One of us (P.J.G.) acknowledges the support of an Alfred P. Sloan research fellowship.

REFERENCES

Baum, W. A., and Code, A. D. (1953). A photometric observation of the occultation of σ Arietis. *Astron. J.* 58, 108–112.

Clifford, A. A. (1973). *Multivariate Error Analysis*. Applied Science Publishers, Essex, England.

Elliot, J. L., and Veverka, J. (1976). Stellar occultation spikes as probes of atmospheric structure and composition. *Icarus* 27, 359–386.

Elliot, J. L., Veverka, J., and Millis, R. L. (1977a). Uranus occults SAO 158687. *Nature* 265, 609.

Elliot, J. L., French, R. G., Dunham, E., Gierasch, P. J., Veverka, J., Church, C., and Sagan, C. (1977b). Occultation of ε Geminorum by Mars. II. The structure and extinction of the Martian upper atmosphere. *Astrophys. J.* 217, 661–679.

French, R. G. (1977). Ph.D. thesis, Cornell University.

Hubbard, W. B., Nather, R. E., Evans, D. S., Tull, R. G., Wells, D. C., van Citters, G. W., Warner, B., and Vanden Bout, P. (1972). The occultation of β Scorpii by Jupiter and Io. I. Jupiter. *Astron. J.* 77, 41–59.

Hunten, D. M., and Veverka, J. (1976). Stellar and spacecraft occultations by Jupiter: A critical review of derived temperature profiles. In *Jupiter* (T. Gehrels, Ed.), pp. 247–283. University of Arizona Press, Tucson.

Jokipii, J. R., and Hubbard, W. H. (1977). Stellar occultations by turbulent planetary atmospheres: The Beta Scorpii events. *Icarus* 30, 537–550.

Kovalevsky, J., and Link, F. (1969). Diamètre aplatissement et propriétes optiques de la haute atmosphere de Neptune d'après l'occultation de l'étoile BD-17° 4388. *Astron. Astrophys.* 2, 398–412.

Pannekoek, A. (1904). Über die Erscheinungen, welche bei einer Sternbedeckung durch einen Planeten auftreten. *Astron. Nachr.* 164, 5–10.

Taylor, G. E. (1976). Oblateness of the atmosphere of Mars. *Nature* 264, 160–161.

Vapillon, L., Combes, M., and Lecacheux, J. (1973). The β Scorpii occultation by Jupiter. II. The temperature and density profiles of the Jovian upper atmosphere. *Astron. Astrophys.* 29, 135–149.

Veverka, J., Wasserman, L. H., Elliot, J. L., Sagan, C., and Liller, W. (1974). The occultation of β Scorpii by Jupiter. I. The structure of the Jovian upper atmosphere. *Astron. J.* 79, 73–84.

Wasserman, L. H., and Veverka, J. (1973). On the reduction of occultation light curves. *Icarus* 20, 322–345.

Young, A. T. (1976). Scintillations during occultations by planets. *Icarus* 27, 335–358.

Icarus 33, 203–209 (1978)

Possible Correlation of Io's Posteclipse Brightening with Major Solar Flares

ROBERT M. NELSON and BRUCE W. HAPKE

Department of Earth and Planetary Sciences, University of Pittsburgh, Pittsburgh, Pennsylvania 15260

Received February 3, 1977; revised May 16, 1977

In 6 of the 7 instances where posteclipse brightening of Io has been reported by observers using blue filters, a major solar flare occurred within 10° of the sub-Jovian longitude in the 100-day interval prior to observation. In none of the 18 instances where no posteclipse brightening was observed did such a flare occur. It is proposed that a phenomenon associated with a major solar flare causes an increase in the trapped particle flux at Io's orbit by an order of magnitude. The posteclipse brightening may be caused by thermoluminescence of Io's surface material upon emergence. Alternatively, it is possible that the increase in trapped particle flux would warm the surface, creating a temporary atmosphere which would precipitate during eclipse cooling and vaporize in the period of warming after reemergence.

INTRODUCTION

In 1964, Binder and Cruikshank reported that Jupiter's innermost Galilean satellite, Io, was brighter by 0.09 magnitudes (~10%) when it emerged from eclipse than 15–20 min later. Since their report, many observers have studied this effect, and both positive and null results are found in the literature. A list of past observations at all wavelength ranges can be found in Frey (1975). To complete Frey's list, the null reports of Nelson (1977) should be included.

Binder and Cruikshank (1964) initially suggested that posteclipse brightening is caused by an atmosphere on Io which precipitates while the satellite is cooling in Jupiter's shadow. Because of later negative reports, succeeding observers have taken great pains to exclude spurious causes, such as scattered light from Jupiter. On no occasion has brightening been reported by one observer and no brightening been reported by another. On at least one occasion brightening was reported by two observers working independently (O'Leary and Veverka, 1971; O'Leary and Minor, 1973). Since competent observers have reported both positive and null results, it is likely that the effect is intermittent. Thus, Cruikshank and Murphy (1973) proposed that the effect is more pronounced at perihelion than at aphelion. They estimated that at perihelion Io's surface temperature is 5% higher than at aphelion, and they suggested that at aphelion the atmosphere is frozen, hence no brightening is observed, while at perihelion, the 5% temperature increase volatilizes the frozen gases which precipitate during eclipse. Sinton (1973) proposed a transient atmosphere for Io that would be frozen at the poles during solstice but would vaporize at equinox. He suggested that the precipitation of this transient atmosphere during eclipse is the cause of posteclipse brightening. Both the perihelion–aphelion hypothesis and the equinox–

0019-1035/78/0331-0203$02.00/0